

Supporting Information

**Enhancement of SOD Activity in Boehmite Supported
Nanoreceptors**

Álvaro Martínez-Camarena, Estefanía Delgado-Pinar, Concepción Soriano,
Javier Alarcón, José M. Llinares, Roberto Tejero, Enrique García-España

Contents

I. Experimental section

II. Figures

Figure S1. ^1H -NMR spectrum of **L1** in D_2O at 298 K.

Figure S2. ^{13}C -NMR spectrum of **L1** in D_2O at 298 K.

Figure S3. Mass spectrum of **L1**.

Figure S4. ^1H -NMR spectra of the three BNP-**L1** samples in D_2O at 298 K.

Figure S5. Calibration and interpolation of **L1** anchoring to boehmite nanoparticles by NMR determination.

Figure S6. Experimental (red, continuous line) and theoretical (discrete red peaks) diffractogram of the boehmite nanoparticles powder.

Figure S7. Size dispersion diagram of the boehmite nanoparticles obtained by DLS.

Figure S8. Distribution diagram of **L1** as a function of the pH in aqueous solution. The UV-vis spectroscopic parameters at 271 nm are overlaid (red dots).

Figure S9. Comparative of the different protonation ways of pyridinol ring and distances in Å of each bond of the ring.

Figure S10. Distribution diagram of the **L1**: Cu^{2+} 1:1 system as a function of the pH in aqueous solution. The UV-vis spectroscopic parameters at 285 nm (red dots) and at 590 nm (green dots) are overlaid.

Figure S11. Cyclic voltammograms at the platinum electrode recorded for **L1** solutions in 50 mM TRIS at pH 7.4: (grey) **L1**, (blue) Cu^{2+} :**L1** 1:1, (red) Cu^{2+} :**L1** 2:1, (yellow) Cu :**L1**-BNP 2:1. Potential scan rate = 50 mV/s.

Figure S12. Distribution diagram of the **L1**/ Zn^{2+} system as a function of the pH in aqueous solution. The UV-vis spectroscopic parameters at 259 nm (red dots) are overlaid.

Figure S13. Distribution diagram of the **L1**/ Cu^{2+} / Zn^{2+} system as a function of the pH in aqueous solution.

III. Tables.

Table S1. Results for the NMR determination of the **L1** anchoring to boehmite nanoparticles.

Table S2. Interpolation and trend lines for the **L1** anchoring determination.

Table S3. Stepwise protonation constants for **L1** obtained by potentiometric measurements. The logarithms constants were determined in 0.15 M NaClO_4 at 298.1 ± 0.1 K.

Table S4. Logarithms of the stability constants of mononuclear and binuclear Cu^{2+} complexes with **L1** obtained by potentiometric measurements. The logarithms constants were determined in 0.15 M NaClO_4 at 298.1 ± 0.1 K.

Table S5. Cartesian coordinates of the Cu^{2+} :**L1** 1:1 optimized complex.

Table S6. Structural data of the Cu^{2+} :**L1** 1:1 optimized complex.

Table S7. Cartesian coordinates of the Cu^{2+} :**L1** 1:2 optimized complex.

Table S8. Structural data of the Cu^{2+} :**L1** 1:2 optimized complex.

Table S9. Logarithms of the stability constants of mononuclear and binuclear Zn^{2+} complexes with **L1** obtained by potentiometric measurements. The logarithms constants were determined in 0.15 M NaClO_4 at 298.1 ± 0.1 K.

Table S10. Logarithms of the stability constants of binuclear Cu^{2+} : Zn^{2+} complexes with **L1** obtained by potentiometric measurements. The logarithms constants were determined in 0.15 M NaClO_4 at 298.1 ± 0.1 K.

Table S11. Apparent formal potential of $\text{Cu}^{2+}/\text{Cu}^+$ couple (E°) from voltammetric data for Cu^{2+} :**L1** 1:1, Cu^{2+} :**L1** 1:2 and Cu^{2+} :**L1**-BNPs 1:2.

IV. References.

I. Experimental section

I.I Synthesis

The synthesis of the compounds 1,5,9,12,16,20-hexakis(p-tolylsulfonyl)-1,5,9,12,16,20-hexaazaeicosane and 4-benzyloxy-2,6-bis(bromomethyl)pyridine were carried out following the procedure described previously in the literature.¹⁻³ All reagents were obtained from commercial sources and used as received. Solvents used for the chemical synthesis were of analytical grade and used without further purification.

1⁴-Benzyloxy-3,7,11,14,18,22-hexakis(p-tolylsulfonyl)-3,7,11,14,18,22-hexaaza-1(2,6)-pyridinacyclotricosaphane (1)⁴⁻⁶

1,5,9,12,16,20-hexakis(p-tolylsulfonyl)-1,5,9,12,16,20-hexaazaeicosane¹ (3.20 g, 2.6 mmol) and K₂CO₃ (6.6 g, 26.4 mmol) were suspended in dried CH₃CN (150 cm³). 4-Benzyloxy-2,6-bis(bromomethyl)pyridine^{2,3} (0.97 g, 3.4 mmol) in 50 cm³ dried CH₃CN was added dropwise to the first mixture, over 3 h. The suspension was refluxed for 24 h and filtered. The solvent of the obtained solution was removed by vacuum evaporation and the resulting oil was purified by column chromatography (SiO₂, CH₂Cl₂:CH₃COCH₃, 97:3). (Yield: 73%) NMR (CDCl₃): δ_H (ppm): 1.81-1.67 (m, 8H), 2.36 (s, 6H), 2.39 (s, 6H), 2.42 (s, 6H), 2.90-3.08 (m, 12H), 3.21 (t, *J*=7.1 Hz, 4H), 3.27 (s, 4H), 4.27 (s, 4H), 5.01 (s, 2H), 6.91 (s, 2H), 7.21-7.44 (m, 17H), 7.56 (d, *J*=8.3 Hz, 4H), 7.66 (dd, *J*=8.3 Hz, 8H). δ_C (ppm): 158.64, 158.54, 143.97, 143.79, 143.73, 136.80, 135.98, 135.34, 130.22, 130.09, 129.08, 128.28, 127.83, 127.63, 127.51, 108.94, 70.36, 54.35, 49.12, 48.42, 48.16, 47.70, 29.56, 29.06, 21.93, 21.88, 21.85. MS *m/z* (ESI) 1444.2 ([M + Na]⁺).

1⁴-Hydroxy-3,7,11,14,18,22-hexaaza-1(2,6)-pyridinacyclotricosaphane (L1·6HCl)⁷

1 (2.74 g, 1.9 mmol) and phenol (16.09 g, 0.17 mol) were suspended in HBr-AcOH 33% (170 cm³). The mixture was stirred at 90 °C for further 48 h and cooled. The resulting suspension was filtered and washed several times with EtOH anhydrous to give the product L1 in a salt form. (Yield: 68%) NMR (D₂O): δ_H (ppm): 2.17-2.39 (m, 8H), 3.27-3.41 (m, 16H), 3.60 (s, 4H), 4.39 (s, 4H), 6.92 (s, 2H). δ_C (ppm): 165.81, 152.45, 110.77, 51.24, 45.28, 45.00, 44.43, 44.06, 43.96, 22.84, 22.72. MS *m/z* (ESI) 408.3 ([M + H]⁺). Anal. Calc. for C₂₂H₄₃ON₇(HCl)₆(H₂O)_{0.5}: C, 37.5; H, 7.4; N, 14.6: Found: C, 37.7; H, 7.6; N, 14.3.

Functionalized nanoparticles with L1

L1·6HCl (134.1 mg, 0.15 mmol) and Na₂CO₃ (143.1 mg, 1.35 mmol) were suspended in EtOH (20 cm³). Boehmite nanoparticles (498.7 mg) were added to the mixture and the resulting suspension was refluxed under Ar atmosphere for 72 h. The resulting mixture were centrifuged and washed several times with a mixture of EtOH (15 cm³), CH₂Cl₂ (5 cm³) and H₂O (2.5 cm³). [L1] = (3.5 ± 0.4) · 10⁻⁵ mol/g_{np-boeh}.

I.II - NMR measurements

The ^1H and ^{13}C NMR spectra were recorded on a Bruker Advance DRX 300 spectrometer operating at 300 MHz for ^1H and at 100.6 MHz for ^{13}C . For the ^{13}C NMR spectra, dioxane was used as a reference standard (δ 67.4 ppm), and for the ^1H spectra, the solvent signal was used.

I.III - Density Functional Theory (DFT) calculations

DFT calculations of the Cu^{2+} complexes were performed with DFT as a computational method using UB3LYP/6-311+G* and UB3LYP/LANDL2DZ combinations. Specifically, the 6-311+G* basis set was used for the nonmetallic atoms, while the LANDL2DZ was used for the transition metals, in which it has been generated ab initio effective core potentials to replace the Coulomb, core orthogonality, and exchange effects of the chemically inert core electrons in Cu^{2+} . The Gaussian 09⁸ package was used for these DFT calculations and the Molden⁹ and Pymol¹⁰ package for the modelling analysis. The aqueous environment was implicitly considered by using the Self-Consistent Reaction Field (SCRF) method with a model of continuous polarization model with water as a solvent (Polarizable Continuum Model or PCM).¹¹⁻¹³

I.IV -In vitro McCord-Fridovich SOD activity assays

SOD-like activity was determined by using the nitro blue tetrazolium (NBT) method.¹⁴⁻¹⁷ The assays were carried out in a pH = 7.4 50 mM HEPES buffer at 298 K. The concentration of NBT was 50 mM and the superoxide was generated with the xanthine oxidase-xanthine system.

I.V- UV-Vis measurements

The solvents used were of spectroscopic or equivalent grade. Water was twice distilled and passed through a Millipore apparatus. The pH values were measured with a Metrohm 713 pH meter and adjustments of the hydrogen ion concentration of the solutions were made with diluted HCl and NaOH solutions. UV-Vis absorption spectra were recorded on an Agilent 8453 spectroscopy system.

I.VI -Electromotive force (EMF) measurements

The potentiometric titrations were carried out at 298.1 ± 0.1 K using 0.15 M NaClO_4 as the supporting electrolyte. The experimental procedure (buret, potentiometer, cell, stirrer, microcomputer, etc.) has been fully described elsewhere.¹⁸ The acquisition of the EMF data was performed with the computer program PASAT.¹⁹ The reference electrode was an Ag/AgCl electrode in a saturated KCl solution. The glass electrode was calibrated as a hydrogen-ion-concentration probe by the titration of previously standardized amounts of HCl with CO_2 free NaOH solutions and the equivalent point determined by the Gran's method,^{20,21} which gives the standard potential, E° , and the ionic product of water [$\text{pK}_w = 13.73(1)$].

The computer program HYPERQUAD was used to calculate the protonation and stability constants.²² The pH range investigated was 2.0–11.0, and the concentrations of Cu^{2+} , Zn^{2+} and the ligand ranged from 1×10^{-3} to 5×10^{-3} mol/dm³,

with Cu^{2+}/L molar ratios varying from 1:1 to 2:1. The different titration curves for each system (at least two) were treated either as a single set or as separated curves without significant variations in the values of the stability constants. Finally, the sets of data were merged together and treated simultaneously to give the final stability constants.

I.VII - Electrochemical Measurements

Cyclic voltammetry experiments were performed with 10^{-3} M aqueous solutions of L1, Cu:L1 (in relation 1:1 and 1:2) and Cu:L1-BNP (in relation 1:2) at pH = 7.4 (50 mM TRIS was used as the buffer). For the study of the electrochemistry of the metal complexes, equimolar amounts of $\text{Cu}(\text{ClO}_4)_2 \cdot 6\text{H}_2\text{O}$ and the ligand were dissolved in 50 mM TRIS, previously degassed, with nitrogen for 10 min, and then the voltammograms were recorded.

Electrochemical experiments were performed with BAS CV 50W and Metrohm PGSTAT 101 Autolab in a conventional three-compartment cell with a glassy-carbon working electrode. Prior to the series of experiments, the working electrode was cleaned and activated. Before each run, the electrode was polished with an aqueous suspension of alumina on a soft surface, dried, and cleaned. AgCl (3 M NaCl)/Ag and a platinum-wire auxiliary electrode completed the three-electrode configuration. The cyclic voltammograms were recorded at scan rates of 10–100 mV/s. The pH was adjusted to the required value by adding appropriate amounts of aqueous HCl and/or NaOH 0.1 M solutions.

I.VIII - Inductively coupled plasma mass spectrometry

Inductively Coupled Plasma - Mass Spectrometry (ICP-MS, 7900, Agilent Technologies) was used for the quantification of the amount of Cu^{2+} complexed to the L1-BNP system.

In a typical experiment an excess of a $\text{Cu}(\text{ClO}_4)_2 \cdot 6\text{H}_2\text{O}$ aqueous solution at pH 7 was added to a known amount of BNPs that contained $(0.35 \pm 0.04) \times 10^{-4}$ mol/g_{BNP} as determined by NMR and elemental microanalysis. According to the distribution diagram (Figure 2), all the grafted ligands might coordinate two Cu^{2+} ions. The pH was increased to 10 to make the BNPs precipitate. Then, the BNPs were washed with water and centrifuged to eliminate the copper excess. Finally, the BNPs were taken to acidic pH to re-disperse them and free the complexed copper. The BNPs were then centrifuged again and the amount of copper in the acidic solution was analysed by ICP-MS. The analysis provided the amount of copper coordinated to the ligand grafted on BNPs. Measurements were made in triplicate. The amount of complexed copper determined was $(0.69 \pm 0.01) \times 10^{-4}$ mol/g_{BNP} supporting that two Cu^{2+} ions were coordinated to each ligand.

II. Figures

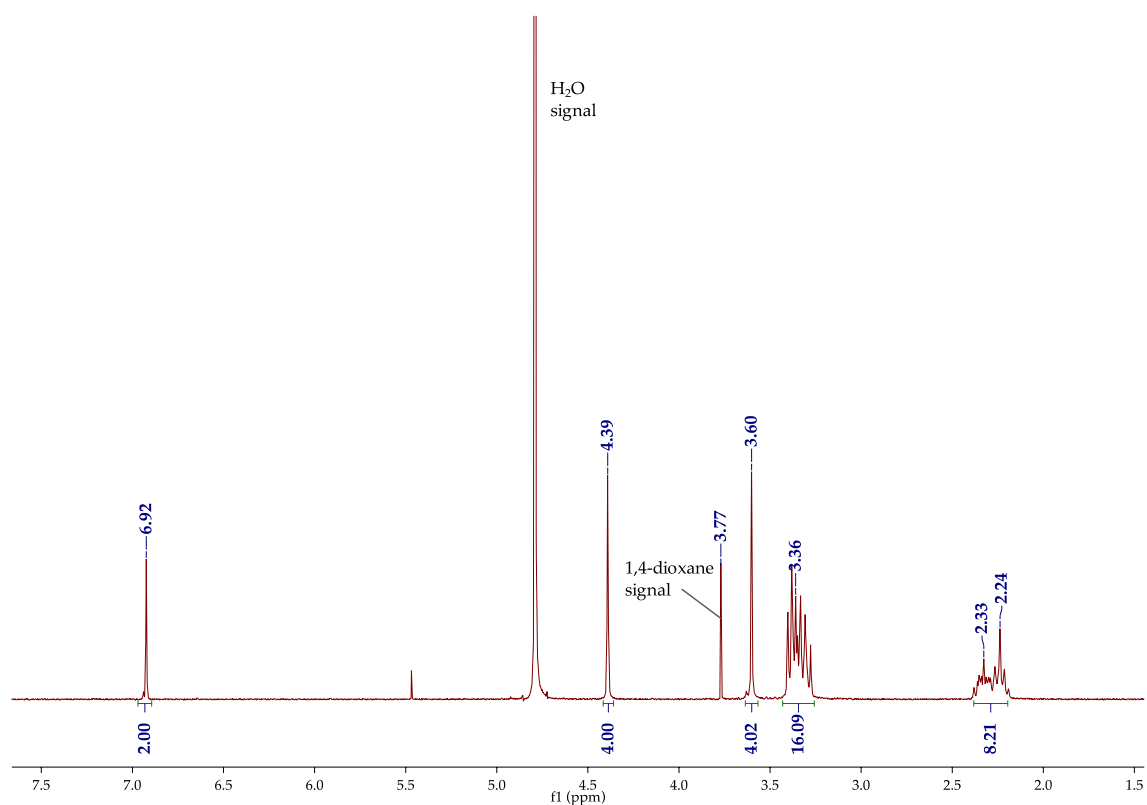


Figure S1. ¹H-NMR spectrum of L1 in D₂O at 298 K.

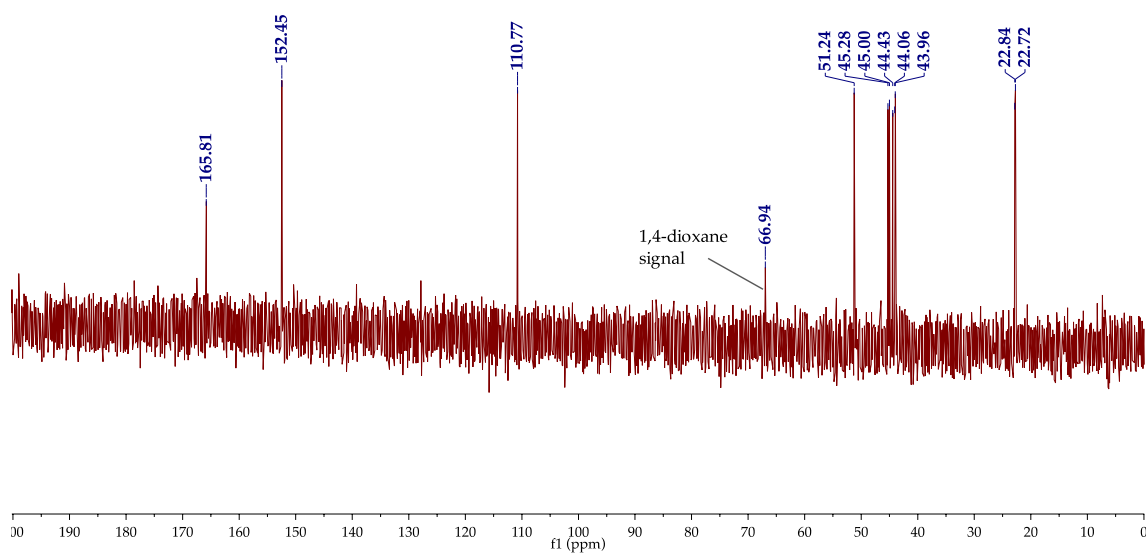


Figure S2. ¹³C-NMR spectrum of L1 in D₂O at 298 K.

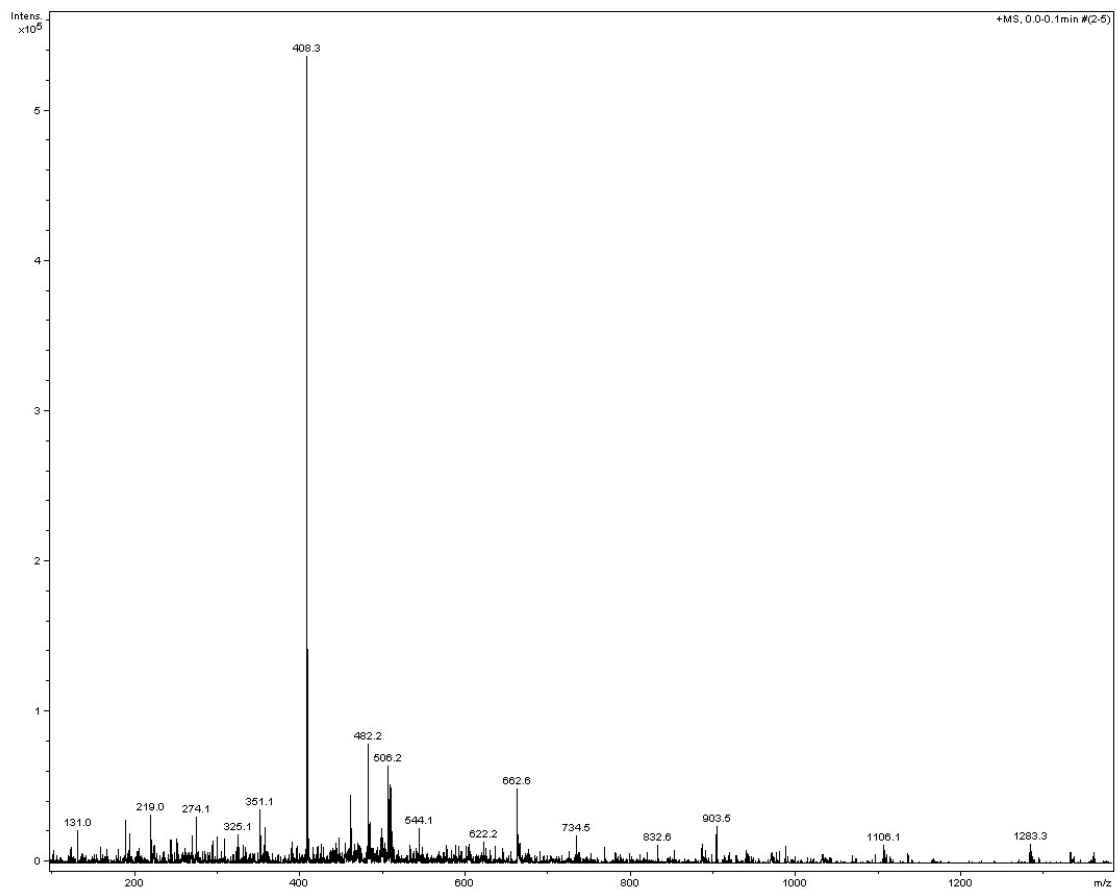


Figure S3. Mass spectrum of L1.

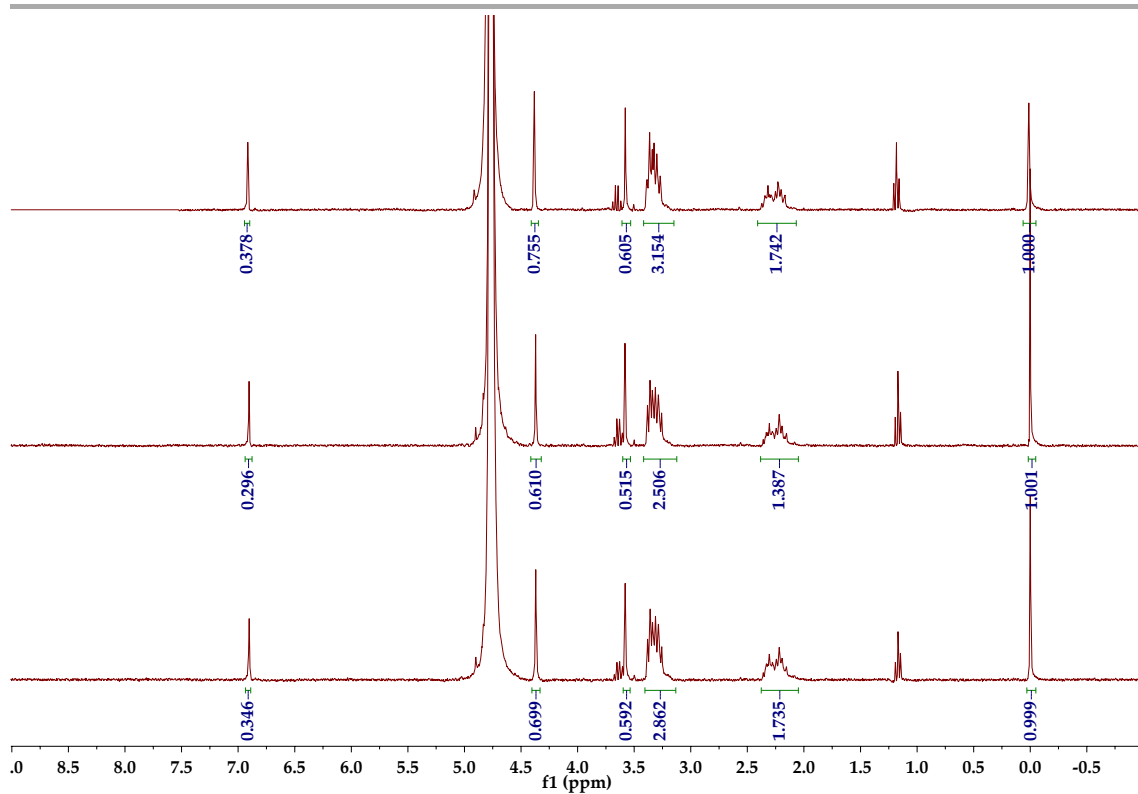


Figure S4. $^1\text{H-NMR}$ spectra of the three BNP-L1 samples in D_2O at 298 K.

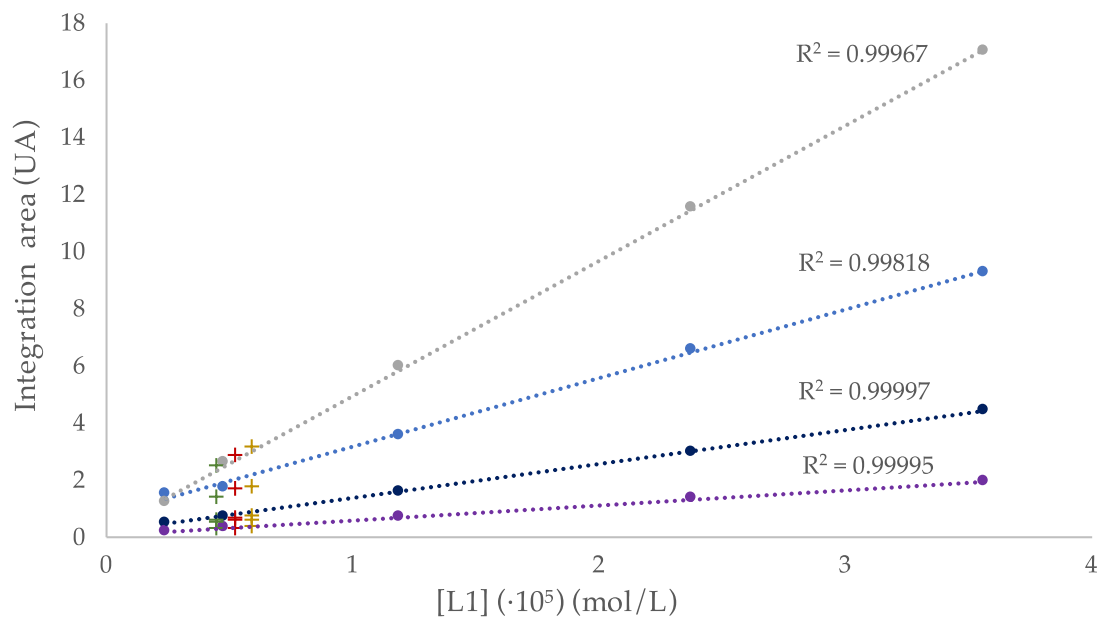


Figure S5. Calibration and interpolation of L1 anchoring to boehmite nanoparticles by NMR determination.

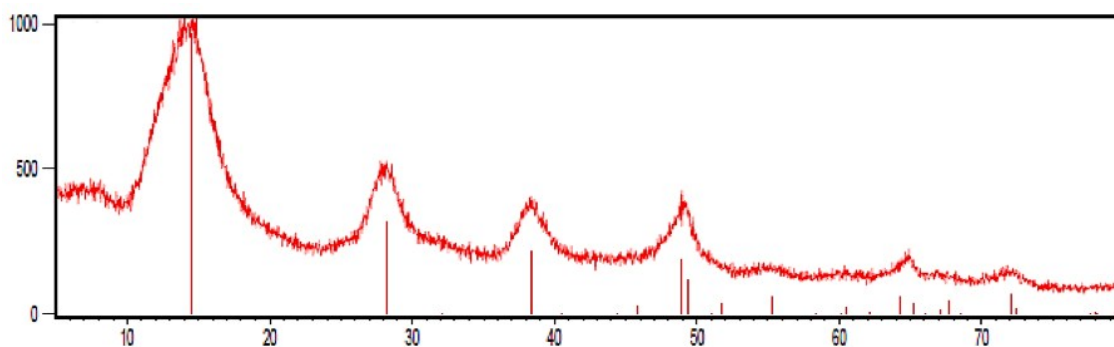


Figure S6. Experimental (red, continuous line) and theoretical (discrete red peaks) diffractogram of the boehmite nanoparticles powder.

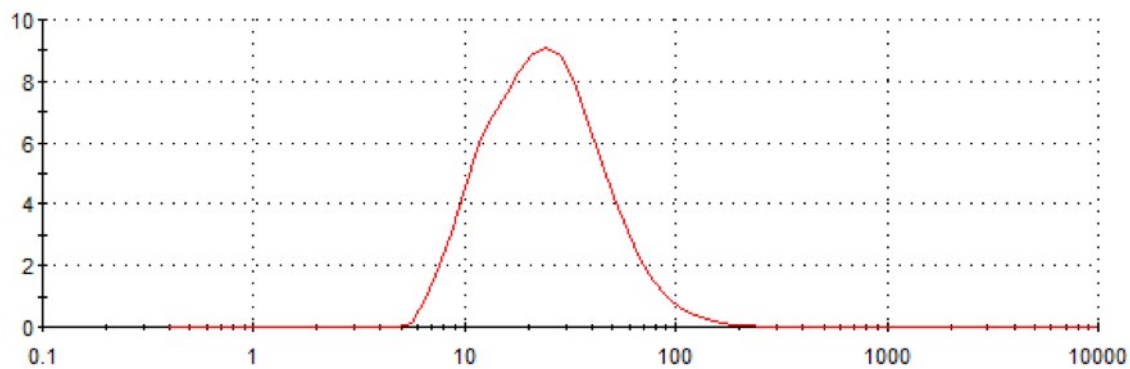


Figure S7. Size dispersion diagram of the boehmite nanoparticles obtained by DLS.

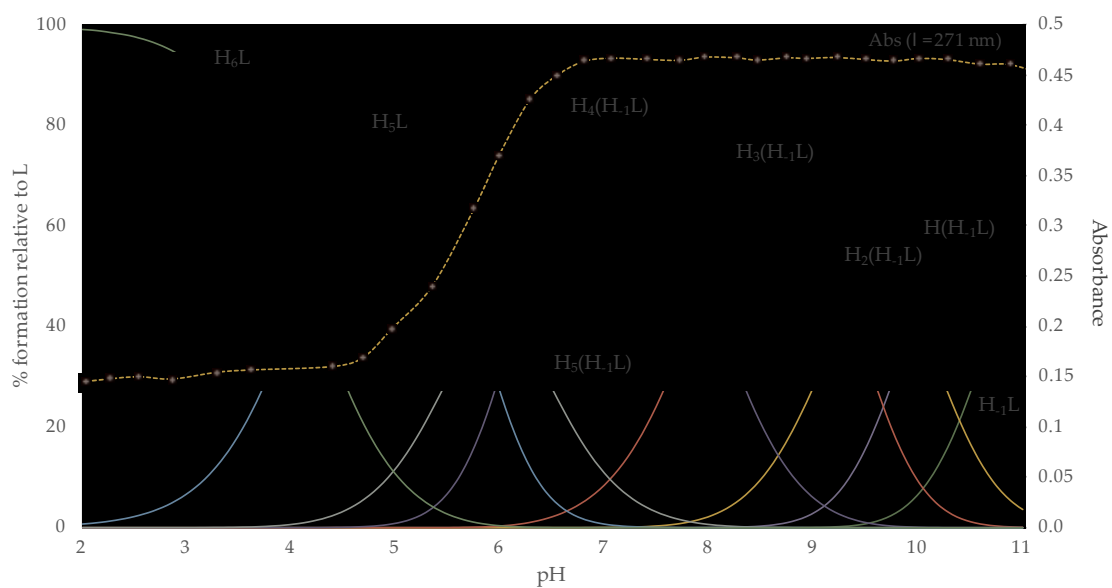


Figure S8. Distribution diagram of **L1** as a function of the pH in aqueous solution. The UV-vis spectroscopic parameters at 271 nm are overlaid (red dots).

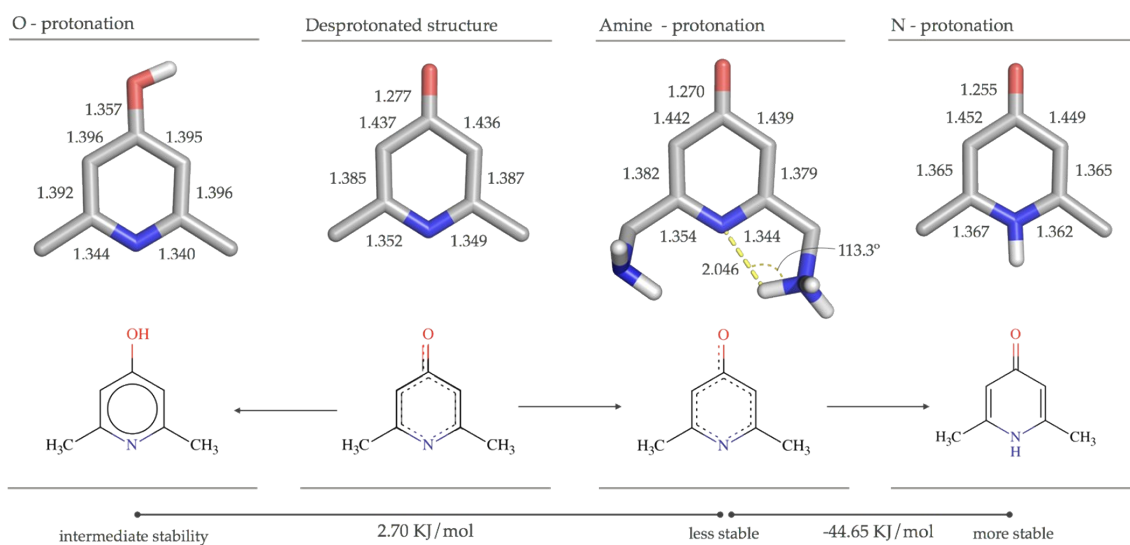


Figure S9. Comparative of the different protonation ways of pyridinol ring and distances in Å of each bond of the ring.

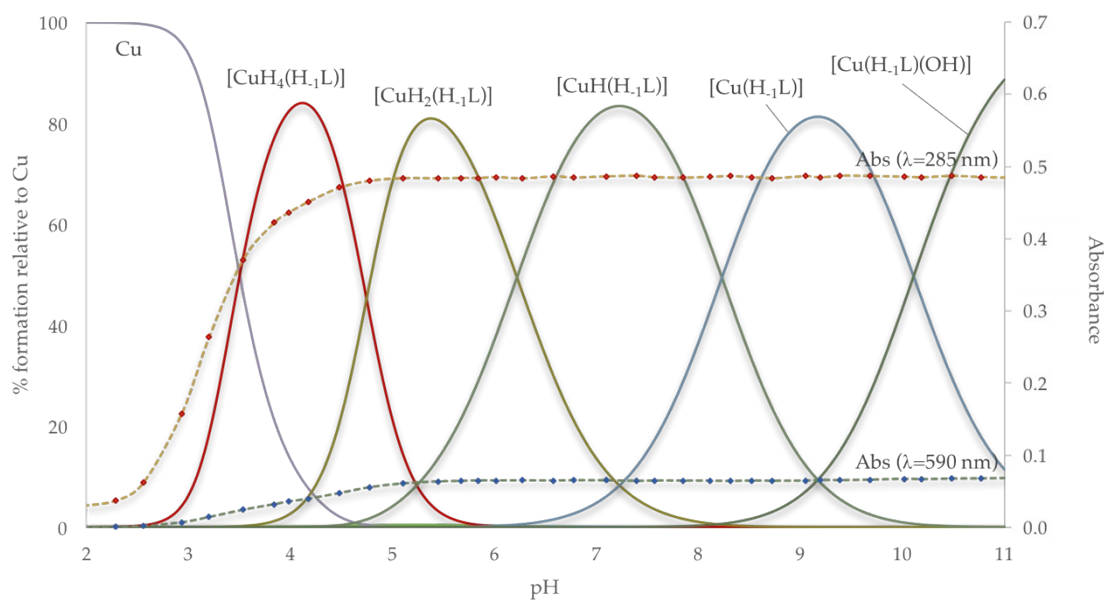


Figure S10. Distribution diagram of the **L1:Cu²⁺** 1:1 system as a function of the pH in aqueous solution. The UV-vis spectroscopic parameters at 285 nm (red dots) and at 590 nm (green dots) are overlaid.

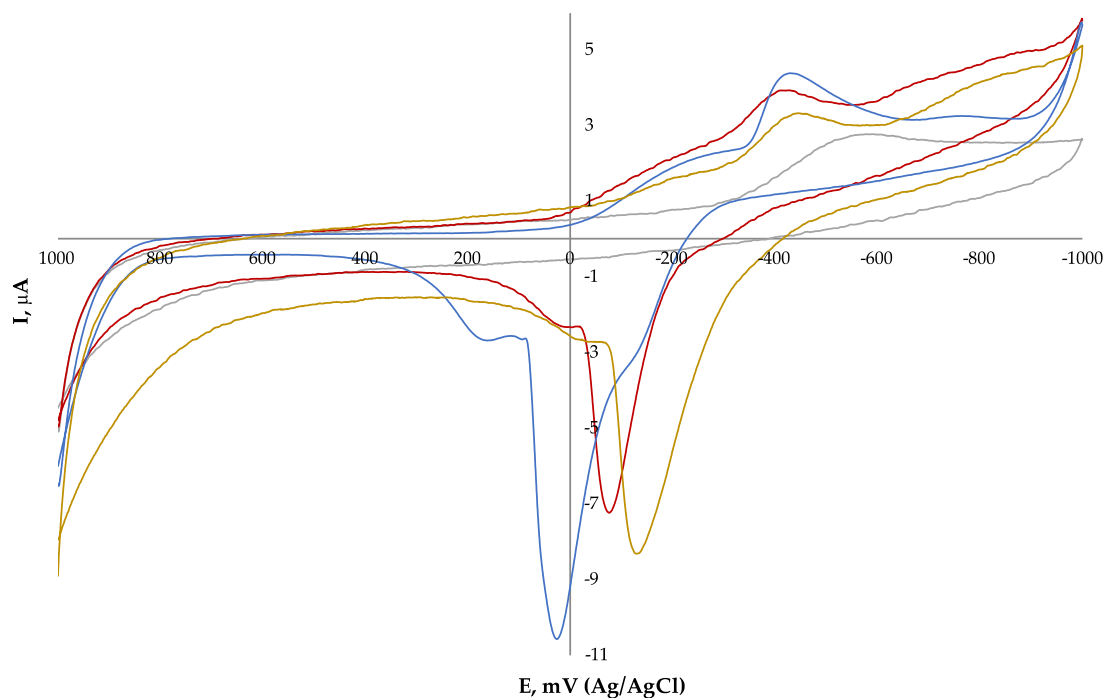


Figure S11. Cyclic voltammograms at the platinum electrode recorded for **L1** solutions in 50 mM TRIS at pH 7.4: (grey) **L1**, (blue) **Cu²⁺:L1** 1:1, (red) **Cu²⁺:L1** 2:1, (yellow) **Cu:L1-BNP** 2:1. Potential scan rate = 50 mV/s.

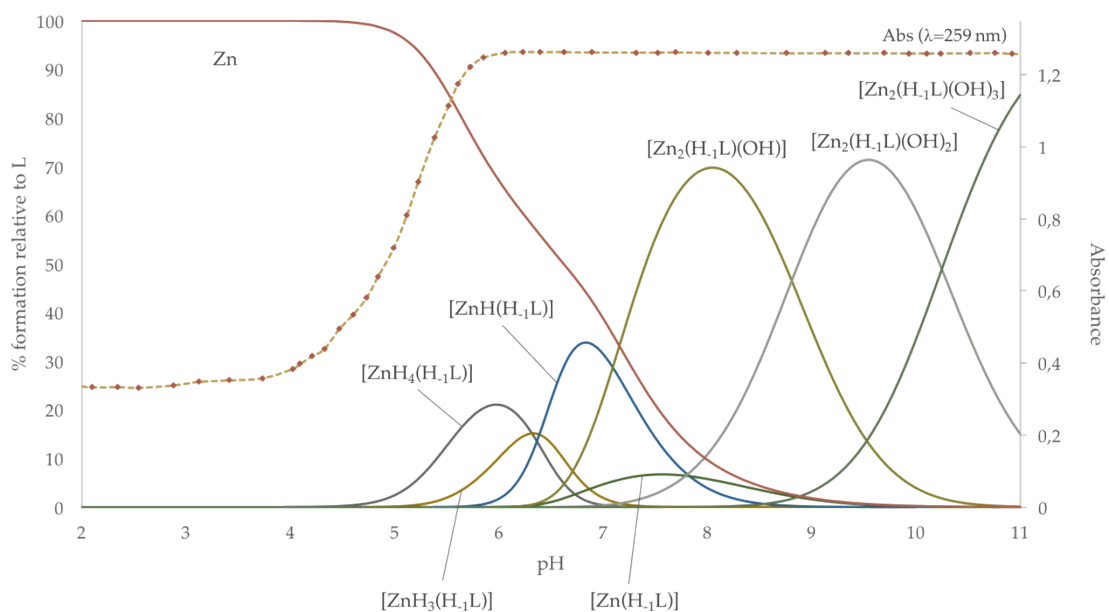


Figure S12. Distribution diagram of the L1/Zn²⁺ system as a function of the pH in aqueous solution. The UV-vis spectroscopic parameters at 259 nm (red dots) are overlaid.

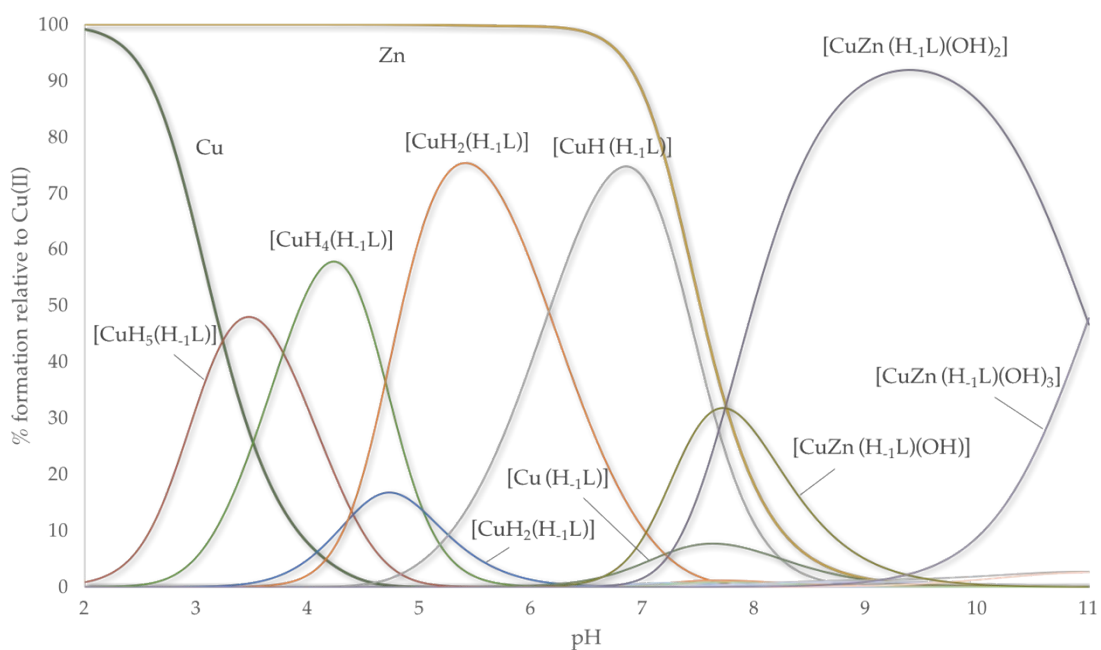


Figure S13. Distribution diagram of the L1/Cu²⁺/Zn²⁺ system as a function of the pH in aqueous solution.

III. Tables

Table S1. Results for the NMR determination of the LI anchoring to boehmite nanoparticles.

Solution	[L] (mol/L)	Area 1	Area 2	Area 3	Area 4	Area 5
Standard 1	4.752·10 ⁻³	12.214	22.667	5.798	5.830	2.606
Standard 2	3.564·10 ⁻³	9.277	17.044	4.423	4.431	1.973
Standard 3	2.376·10 ⁻³	6.545	11.550	2.992	3.020	1.353
Standard 4	1.188·10 ⁻³	3.592	5.989	1.580	1.616	0.709
Standard 5	0.475·10 ⁻³	1.701	2.601	0.748	0.720	0.330
Sample 1	-	1.742	3.154	0.605	0.755	0.378
Sample 2	-	1.387	2.506	0.515	0.610	0.296
Sample 3	-	1.735	2.862	0.592	0.699	0.346

Table S2. Interpolation and trend lines for the LI anchoring determination.

Signal	Equation	R ²
Area 1	Int. = 2440.7·[L] + 0.6353	0.99961
Area 2	Int. = 4683.0·[L] + 0.3996	0.99998
Area 3	Int. = 1184.5·[L] + 0.1816	0.99996
Area 4	Int. = 1191.8·[L] + 0.1786	0.99992
Area 5	Int. = 532.1·[L] + 0.0795	0.99997

Table S3. Stepwise protonation constants for *L1* obtained by potentiometric measurements. The logarithms constants were determined in 0.15 M NaClO₄ at 298.1 ± 0.1 K.

Entry	Reaction	L1
1	$H_{-1}L^{-} + H^{+} \rightleftharpoons H(H_{-1}L)$	10.68(2) ^a
2	$H(H_{-1}L) + H^{+} \rightleftharpoons H_2(H_{-1}L)^{+}$	10.11(2)
3	$H_2(H_{-1}L)^{+} + H^{+} \rightleftharpoons H_3(H_{-1}L)^{2+}$	9.36(1)
4	$H_3(H_{-1}L)^{2+} + H^{+} \rightleftharpoons H_4(H_{-1}L)^{3+}$	7.97(1)
5	$H_4(H_{-1}L)^{3+} + H^{+} \rightleftharpoons H_5(H_{-1}L)^{4+}$	6.13(1)
6	$H_5(H_{-1}L)^{4+} + H^{+} \rightleftharpoons H_5L^{4+}$	5.81(1)
7	$H_5L^{4+} + H^{+} \rightleftharpoons H_6L^{5+}$	4.14(2)
8	Log β^b	54.20

^a Values in parentheses are standard deviations in the last significant figure.

^b $\text{Log } \beta = \sum \log K$

Table S4. Logarithms of the stability constants of mononuclear and binuclear Cu²⁺ complexes with *L1* obtained by potentiometric measurements. The logarithms constants were determined in 0.15 M NaClO₄ at 298.1 ± 0.1 K.

Entry	Reaction	L1
1	$[CuH_4(H_{-1}L)]^{5+} + H^{+} \rightleftharpoons [CuH_5(H_{-1}L)]^{6+}$	3.79(6) ^a
2	$[CuH_3(H_{-1}L)]^{4+} + H^{+} \rightleftharpoons [CuH_4(H_{-1}L)]^{5+}$	5.04(7)
3	$[CuH_2(H_{-1}L)]^{3+} + H^{+} \rightleftharpoons [CuH_3(H_{-1}L)]^{4+}$	4.35(7)
4	$[CuH(H_{-1}L)]^{2+} + H^{+} \rightleftharpoons [CuH_2(H_{-1}L)]^{3+}$	6.16(4)
5	$[Cu(H_{-1}L)]^{+} + H^{+} \rightleftharpoons [CuH(H_{-1}L)]^{2+}$	8.24(4)
6	$H_{-1}L^{-} + Cu(II) \rightleftharpoons [Cu(H_{-1}L)]^{+}$	23.56(4)
7	$[Cu(H_{-1}L)]^{+} + H_2O \rightleftharpoons [Cu(H_{-1}L)(OH)] + H^{+}$	-10.11(5)
8	$[Cu(H_{-1}L)]^{+} + Cu(II) \rightleftharpoons [Cu_2(H_{-1}L)]^{3+}$	8.80(4)
9	$[Cu_2(H_{-1}L)]^{3+} + H_2O \rightleftharpoons [Cu_2(H_{-1}L)(OH)]^{2+} + H^{+}$	-7.26(6)
10	$[Cu_2(H_{-1}L)(OH)]^{2+} + H_2O \rightleftharpoons [Cu_2(H_{-1}L)(OH)_2]^{+} + H^{+}$	-8.20(6)
11	$Cu(II) + H(H_{-1}L) \rightleftharpoons [CuH(H_{-1}L)]^{2+}$	21.11(4)
12	$2Cu(II) + H(H_{-1}L) \rightleftharpoons [Cu_2H(H_{-1}L)]^{4+}$	26.44(4)
13	$[CuH(H_{-1}L)]^{2+} + Cu(II) \rightleftharpoons [Cu_2H(H_{-1}L)]^{4+}$	5.33(4)

^a Values in parentheses are standard deviations in the last significant figure.

Table S5. Cartesian coordinates of the **L1:Cu²⁺** 1:1 optimized complex.

Atom	X	Y	Z
C	-0.244	-0.418	0.217
C	-0.148	-0.320	1.596
C	2.203	-0.303	0.106
C	2.220	-0.187	1.486
N	1.064	-0.196	2.241
O	0.894	-0.509	-1.918
C	-1.315	-0.416	2.551
N	-0.999	0.315	3.829
C	3.472	-0.022	2.319
N	3.179	-0.493	3.711
C	-1.447	1.754	3.845
C	-0.717	2.706	2.880
C	0.806	2.918	3.107
N	1.239	2.573	4.507
C	4.257	-0.220	4.718
C	3.687	-0.055	6.143
C	2.593	-1.072	6.523
N	1.202	-0.568	6.190
C	0.660	3.538	5.525
C	1.696	4.423	6.253
C	2.229	3.787	7.560
N	1.111	3.498	8.473
C	0.163	-1.633	6.530
C	-1.143	-1.060	7.117
C	-0.998	-0.363	8.485
N	-0.152	0.857	8.379
C	1.297	2.504	9.547

C	0.066	1.587	9.660
H	-1.222	-0.518	-0.262
H	3.141	-0.320	-0.458
H	-1.491	-1.475	2.815
H	-2.246	-0.027	2.098
H	-1.469	-0.166	4.609
H	3.765	1.042	2.387
H	4.326	-0.572	1.880
H	2.970	-1.503	3.684
H	-1.330	2.101	4.883
H	-2.530	1.782	3.604
H	-1.245	3.674	2.975
H	-0.876	2.382	1.834
H	1.058	3.972	2.857
H	1.379	2.272	2.424
H	2.268	2.633	4.549
H	4.777	0.704	4.416
H	4.996	-1.044	4.693
H	4.527	-0.139	6.856
H	3.279	0.967	6.262
H	2.627	-1.275	7.611
H	2.740	-2.041	6.012
H	1.003	0.223	6.857
H	0.105	2.981	6.300
H	-0.065	4.184	4.998
H	2.541	4.674	5.581
H	1.216	5.387	6.513
H	3.007	4.457	7.996
H	2.733	2.827	7.339
H	0.633	4.348	8.792

H	-1.624	-0.349	6.417
H	-1.854	-1.900	7.225
H	-0.507	-1.049	9.201
H	-2.013	-0.144	8.89
H	-0.544	1.523	7.697
CU	1.119	0.110	4.203
C	0.946	-0.413	-0.628
H	0.21	0.855	10.47
H	-0.827	2.191	9.939
H	2.171	1.878	9.291
H	1.503	2.967	10.54
H	0.606	-2.321	7.278
H	-0.041	-2.228	5.623

Table S6. Structural data of the **L1:Cu²⁺ 1:1** optimized complex.

Atoms	Distance (Å)	Atoms	Angle (°)
Cu-N1	1.986	N1-Cu-N2	79.4
Cu-N2	2.161	N1-Cu-N3	106.0
Cu-N3	2.485	N1-Cu-N4	152.3
Cu-N4	2.101	N1-Cu-N5	76.3
Cu-N5	2.202	N2-Cu-N3	88.5
		N2-Cu-N4	103.5
		N2-Cu-N5	154.7
		N3-Cu-N4	101.7
		N3-Cu-N5	104.7
		N4-Cu-N5	94.9

Table S7. Cartesian coordinates of the Cu^{2+} : **L1** 1:2 optimized complex.

Atom	X	Y	Z
C	-5.305	0.165	-1.018
C	-3.951	-0.041	-1.151
C	-4.861	1.217	1.126
C	-3.529	0.968	0.918
N	-3.082	0.319	-0.185
O	-7.091	0.984	0.326
C	-3.318	-0.643	-2.399
N	-1.841	-0.765	-2.274
C	-2.399	1.416	1.824
N	-1.241	1.706	0.944
C	-1.273	-2.106	-2.566
C	-1.855	-3.259	-1.732
C	-2.278	-2.969	-0.285
N	-1.320	-2.180	0.513
C	0.004	2.150	1.599
C	0.790	3.040	0.625
C	2.311	3.057	0.785
N	3.02	2.014	-0.023
C	-0.03	-2.862	0.706
C	0.715	-2.258	1.893
C	2.189	-2.630	1.990
N	3.080	-1.921	1.014
C	4.470	2.382	-0.126
C	5.395	1.268	-0.626
C	4.831	0.453	-1.789
N	3.834	-0.541	-1.302
C	3.433	-2.695	-0.205

C	4.418	-1.876	-1.020
H	-5.984	-0.128	-1.813
H	-5.191	1.755	2.010
H	-3.565	-0.016	-3.260
H	-3.758	-1.621	-2.604
H	-1.414	-0.116	-2.927
H	-2.125	0.618	2.521
H	-2.688	2.294	2.413
H	-1.546	2.442	0.302
H	-0.201	-2.013	-2.381
H	-1.394	-2.350	-3.629
H	-1.112	-4.062	-1.749
H	-2.734	-3.677	-2.233
H	-2.473	-3.935	0.202
H	-3.223	-2.425	-0.271
H	-1.755	-2.051	1.428
H	0.576	1.270	1.890
H	-0.220	2.707	2.517
H	0.431	4.068	0.728
H	0.548	2.745	-0.399
H	2.609	2.929	1.826
H	2.689	4.030	0.457
H	2.632	2.061	-0.968
H	0.548	-2.750	-0.210
H	-0.175	-3.940	0.874
H	0.232	-2.580	2.822
H	0.618	-1.170	1.859
H	2.33	-3.709	1.875
H	2.553	-2.371	2.985
H	3.955	-1.768	1.512

H	4.798	2.708	0.861
H	4.542	3.250	-0.790
H	6.333	1.736	-0.935
H	5.655	0.592	0.194
H	5.634	-0.068	-2.318
H	4.343	1.102	-2.517
H	3.108	-0.663	-2.003
CU	-1.147	-0.015	-0.320
CU	2.707	0.036	0.427
O	-2.782	-1.833	3.176
H	-3.736	-1.688	3.149
O	1.587	1.756	-2.771
H	1.886	1.440	-3.633
H	0.968	2.474	-2.957
O	0.799	-0.070	-0.543
H	0.962	0.439	-1.352
H	-2.624	-2.450	3.901
C	-5.851	0.792	0.161
O	-2.372	3.813	-0.870
H	-2.075	4.731	-0.868
H	-3.336	3.840	-0.907
O	2.97	0.536	2.571
H	2.398	0.350	3.326
H	3.856	0.689	2.922
H	5.344	-1.730	-0.458
H	4.676	-2.392	-1.949
H	2.525	-2.886	-0.776
H	3.871	-3.661	0.064

Table S8. Structural data of the $\text{Cu}^{2+}:\text{L1}$ 1:2 optimized complex.

Atoms	Distance (Å)	Atoms	Angle (°)
Cu1-N1	2.137	N1-Cu1-N2	77.3
Cu1-N2	1.968	N1-Cu1-N3	141.6
Cu1-N3	2.205	N1-Cu1-N4	122.3
Cu1-N4	2.326	N1-Cu1-O1	97.7
Cu1-O1	1.960	N2-Cu1-N3	79.0
Cu2-N5	2.077	N2-Cu1-N4	93.5
Cu2-N6	2.143	N2-Cu1-O1	171.5
Cu2-N7	2.053	N3-Cu1-N4	88.7
Cu2-O1	2.143	N3-Cu1-O1	101.7
Cu2-O2	2.217	N4-Cu1-O1	95.1
		N5-Cu2-N6	83.1
		N5-Cu2-N7	160.5
		N5-Cu2-O1	104.0
		N5-Cu2-O2	85.3
		N6-Cu2-N7	90.1
		N6-Cu2-O1	95.1
		N6-Cu2-O2	141.1
		N7-Cu2-O1	94.8
		N7-Cu2-O2	88.7
		O1-Cu2-O2	123.7

Table S9. Logarithms of the stability constants of mononuclear and binuclear Zn^{2+} complexes with **L1** obtained by potentiometric measurements. The logarithms constants were determined in 0.15 M $NaClO_4$ at 298.1 ± 0.1 K.

Entry	Reaction	L1
1	$[ZnH_2(H_{-1}L)]^{3+} + H^+ \rightleftharpoons [ZnH_3(H_{-1}L)]^{5+}$	6.32(3) ^a
2	$[Zn(H_{-1}L)]^{2+} + 2H^+ \rightleftharpoons [ZnH_2(H_{-1}L)]^{4+}$	12.78(2)
3	$H(H_{-1}L) + Zn(II) \rightleftharpoons [ZnH(H_{-1}L)]^{2+}$	11.80(1)
4	$H_{-1}L^- + Zn(II) \rightleftharpoons [Zn(H_{-1}L)]^+$	14.65(2)
5	$[Zn(H_{-1}L)]^+ + H_2O \rightleftharpoons [Zn(H_{-1}L)(OH)] + H^+$	-9.96(3)
6	$[Zn(H_{-1}L)(OH)] + H_2O \rightleftharpoons [Zn(H_{-1}L)(OH)_2]^- + H^+$	-10.92(3)
7	$2Zn(II) + H_{-1}L^- + H_2O \rightleftharpoons [Zn_2(H_{-1}L)(OH)]^{2+} + H^+$	11.14(3)
8	$[Zn_2(H_{-1}L)(OH)]^{2+} + H_2O \rightleftharpoons [Zn_2(H_{-1}L)(OH)_2]^+ + H^+$	-8.81(3)
9	$[Zn_2(H_{-1}L)(OH)_2]^+ + H_2O \rightleftharpoons [Zn_2(H_{-1}L)(OH)_3] + H^+$	-10.26(4)

^a Values in parentheses are standard deviations in the last significant figure.

Table S10. Logarithms of the stability constants of binuclear $Cu^{2+}:Zn^{2+}$ complexes with **L1** obtained by potentiometric measurements. The logarithms constants were determined in 0.15 M $NaClO_4$ at 298.1 ± 0.1 K.

Reaction	L1
$Cu(II) + Zn(II) + H_{-1}L^- + H_2O \rightleftharpoons [CuZn(H_{-1}L)(OH)]^{2+} + H^+$	19.93(5) ^a
$Cu(II) + Zn(II) + H_{-1}L^- + 2H_2O \rightleftharpoons [CuZn(H_{-1}L)(OH)_2]^+ + H^+$	12.19(3)
$Cu(II) + Zn(II) + H_{-1}L^- + 3H_2O \rightleftharpoons [CuZn(H_{-1}L)(OH)_3] + H^+$	1.20(7)

^a Values in parentheses are standard deviations in the last significant figure.

Table S11. Apparent formal potential of Cu^{2+}/Cu^+ couple ($E^{\circ'}$) from voltammetric data for $Cu^{2+}:\mathbf{L1}$ 1:1, $Cu^{2+}:\mathbf{L1}$ 1:2 and $Cu^{2+}:\mathbf{L1}$ -BNPs 1:2.

	IC ₅₀ (μM)	$E^{\circ'}$ (mV vs SCE)	Reference
Cu ₂ L1	0.8(1)	-158 ± 5	This work
CuL1	1.4(5)	-54 ± 5	This work
Cu ₂ L1-BNPs	0.10(3)	-223 ± 5	This work
Cu ₂ L2	1.2(2)b	-150 ± 5	Ref. 1
Cu ₂ Zn ₂ SOD	0.010(2)b	+76	Ref. 23

IV. References

- 1 R. Belda, S. Blasco, B. Verdejo, H. R. Jiménez, A. Doménech-Carbó, C. Soriano, J. Latorre, C. Terencio and E. García-España, *Dalton Trans.*, 2013, **42**, 11194–204.
- 2 E. Busto, A. González-Álvarez, V. Gotor-Fernández, I. Alfonso and V. Gotor, *Tetrahedron*, 2010, **66**, 6070–6077.
- 3 P. Froidevaux, J. M. Harrowfield and A. N. Sobolev, *Inorg. Chem.*, 2000, **39**, 4678–4687.
- 4 J. E. Richman and T. J. Atkins, *J. Am. Chem. Soc.*, 1974, **96**, 2268–2270.
- 5 J. E. Richman, T. J. Atkins and W. T. Oettle, *Organic Synthesis, volumen VI*, John Wiley & Sons, Inc, 1988.
- 6 B. L. Shaw, *J. Am. Chem. Soc.*, 1975, **97**, 3856–3857.
- 7 B. E. Haskell and S. B. Bowlus, *J. Org. Chem.*, 1976, **41**, 159–160.
- 8 M. J. Frisch, G. W. Trucks, H. B. Schlegel, G. E. Scuseria, M. A. Robb, J. R. Cheeseman, G. Scalmani, V. Barone, B. Mennucci, G. A. Petersson, H. Makatsuji, M. Caricato, X. Li, H. P. Hratchian, A. F. Izmaylov, J. Bloino, G. Zheng, J. L. Sonnenberg and M. Hada, 2009.
- 9 G. Schaftenaar and J. H. Noordik, *J. Comput. Mol. Des.*, 2000, **14**, 123–134.
- 10 Schrodinger LLC, 2015.
- 11 S. Miertuš, E. Scrocco and J. Tomasi, *Chem. Phys.*, 1981, **55**, 117–129.
- 12 J. L. Pascual-ahuir, E. Silla and I. Tuñón, *J. Comput. Chem.*, 1994, **15**, 1127–1138.
- 13 M. Cossi, G. Scalmani, N. Rega and V. Barone, *J. Chem. Phys.*, 2002, **117**, 43–54.
- 14 L. W. Oberley and D. R. Spitz, *Oxygen Radicals in Biological Systems*, Elsevier, 1984, vol. 105.
- 15 L. W. Oberley and D. R. Spitz, *Handbook of methods of oxygen radicals research*, CRC Press, Boca Raton, USA, 1986.
- 16 C. Beauchamp and I. Fridovich, *Anal. Biochem.*, 1971, **44**, 276–287.
- 17 J. Y. Zhou and P. Prognon, *J. Pharm. Biomed. Anal.*, 2006, **40**, 1143–8.
- 18 E. Garcia-Espana, M. J. Ballester, F. Lloret, J. M. Moratal, J. Faus and A. Bianchi, *J. Chem. Soc. Dalt. Trans. Inorg. Chem.*, 1988, **2**, 101–104.
- 19 M. Fontanelli and M. Micheloni, 1990.
- 20 G. Gran, *Analyst*, 1952, **77**, 661–671.
- 21 F. J. C. Rossotti and H. Rossotti, *J. Chem. Educ.*, 1965, **42**, 375.
- 22 P. Gans, A. Sabatini and A. Vacca, *Talanta*, 1996, **43**, 1739–1753.
- 23 H. Ohtsu, Y. Shimazaki, A. Odani, O. Yamauchi, W. Mori, S. Itoh and S. Fukuzumi, *J. Am. Chem. Soc.*, 2000, **122**, 5733–5741.